www.acsnano.org

# Direct Observation of Emulsion Morphology, Dynamics, and Demulsification

Maria A. Vratsanos and Nathan C. Gianneschi\*



Downloaded via UNIV OF CONNECTICUT on November 4, 2022 at 18:13:39 (UTC). See https://pubs.acs.org/sharingguidelines for options on how to legitimately share published articles.

Cite This: ACS Nano 2022, 16, 7783-7793



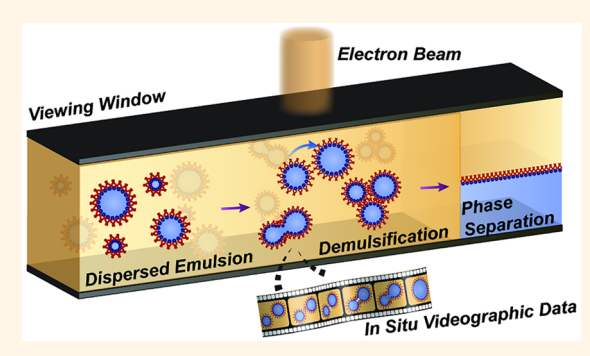
**ACCESS** 

Metrics & More

Article Recommendations

Supporting Information

ABSTRACT: Herein, we present the direct observation and quantification of a water-in-oil (w/o) emulsion, its destabilization, and the effect of additives on such processes at the nanoscale. This is achieved via liquid phase transmission electron microscopy (LPTEM), wherein a small volume of emulsion is encapsulated against vacuum in its liquid state to allow observation of its initial morphology and its evolution over time at excellent spatial and temporal resolution. Emulsions of this class are useful for delivering payloads of materials insoluble in their delivery medium and are currently widely used across food science, pharmaceuticals, and environmental applications. However, their utility is inherently limited by their thermodynamic tendency to demulsify, eventually leading to bulk phase separation. This occurs via several



degradation mechanisms, operating at times collectively, and which are difficult to differentiate *via* traditional ensemble methods (e.g., light scattering), obscuring mechanistic nuances. LPTEM as a characterization technique has the potential to augment our understanding of emulsion behavior and improve performance and formulations. In this work, we also emphasize the importance of the included videographic Supporting Information data in demonstrating the behavior of the studied materials.

KEYWORDS: emulsions, surfactants, phase separation, droplet dynamics, liquid phase TEM

#### **INTRODUCTION**

Emulsions are defined as dispersions of two or more immiscible liquids and found with utility everywhere from the human gastrointestinal tract, to condiments, to many common cosmetics. Due to the desire to minimize the contact surface area between two immiscible substances, emulsions are thermodynamically unstable and will eventually completely phase separate.<sup>2</sup> However, surface active agents, or surfactants,<sup>3</sup> may be employed to slow this separation and stabilize the emulsion for longer periods of time. Surfactants are amphiphilic molecules having moieties soluble in both phases, which lowers the interfacial tension so as to allow droplet formation of one phase in the other. There exists an extensive library of classes of surfactant molecules, each with their own respective advantages. However, the commonality among these materials is that for most industrial applications, there is significant interest in minimizing the amount of surfactant included in the formulation.<sup>5</sup> While increasing surfactant content generally extends shelf life, it may also have significant effects on other properties of the substance, such as changing its taste or texture, or causing adverse reactions when used to formulate therapeutics, and may be environmentally detrimental.<sup>5-8</sup> Generally, then, there exists a need to optimize formulations with respect to both maximal shelf life and

judicious choice of surfactant type and concentration. To achieve this, analytical methods are needed that provide an understanding of how emulsions degrade and how this is influenced by surfactants and other additives. To that end, for a given system, fundamental knowledge of the various degradation pathways and emulsion behavior is valuable (Figure 1).

Emulsion characterization is currently almost entirely dependent on ensemble methods such as light scattering 9-11 and rheology. 2,6,12,13 While these powerful techniques provide information about global populations (such as size distributions and time scales), the inability to directly observe emulsion morphology and behavior at the nanoscale leaves many questions unanswered, especially with regard to demulsification. There are three main pathways for emulsion degradation progressing from an initial dispersed state: coalescence, flocculation, and Ostwald ripening. Emulsions

Received: January 7, 2022 Accepted: March 2, 2022 Published: March 18, 2022





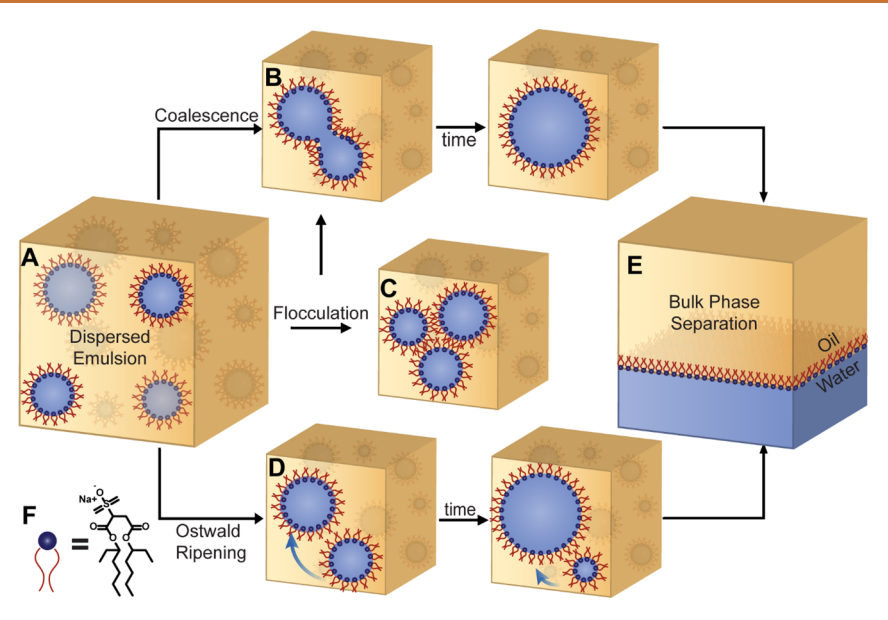


Figure 1. Overview of demulsification pathways. Emulsions begin as dispersed droplets of one immiscible phase in a continuous one, shown here (A) as a water-in-oil dispersion. Emulsions will experience (B) coalescence, (C) flocculation, and/or (D) Ostwald ripening in time, eventually leading to (E) bulk phase separation. (F) Surfactant molecules are represented by blue and red shapes, with the structure of AOT as shown.

exhibit these processes, either sequentially or concurrently, to eventually yield a completely phase separated system (Figure 1A-E). 14-21 At various times, the field has focused on either Ostwald ripening or coalescence as the predominant pathway, but it is becoming clear that the relative contributions of each are largely system dependent, both with respect to phases and surfactants (Figure 1F).<sup>22</sup> However, scattering techniques are insufficient to disentangle the details of multiple processes and are unable to distinguish between the various pathways over time.<sup>23</sup> Further, conclusions drawn from scattering data regarding the kinetics of such processes are based on constitutive models. In Ostwald ripening, many of these predictions are predicated on Lifshitz-Slezov-Wagner (LSW) theory, which was originally derived for particles in a solid matrix, but has been applied with moderate accuracy to oil-inwater (o/w) emulsions. 10,14,24,25 Studies of its application to water-in-oil (w/o) systems have shown deviation from predicted behavior at longer time points (in part attributable to the slower kinetics of the greater molar volume of the solute phase) and have noted its failure to account for the presence of surfactant micelles, as well as its disregard for the effects of droplet concentration. 6,26 Thus, conclusions made regarding emulsions predicated on this theory may not hold true, especially in cases of nanoemulsions. That is, having droplets <200 nm removes sedimentation as a confounding mechanism of degradation, making the understanding of the processes at play even more critical.<sup>14</sup> Further, recent models have demonstrated that individual droplets may significantly deviate from predicted Fickian behavior, undergoing anomalous diffusion due to complex mass transfer processes.<sup>16</sup> In this view, ensemble characterization can miss the mark by relying on statistical averaging that destroys the nuances of the process, especially given the reliance of dynamic light scattering on the assumption of Brownian motion.<sup>27</sup> Measurements of optical transmission over time are used to indirectly determine whether Ostwald ripening is occurring, as optical transparency may qualitatively indicate the degree of dispersity of the droplets. However, this takes a rather coarse view of the

process and is easily skewed, as the appearance of even a small population of micrometer-scale droplets will influence these measurements. Thus, there is a distinct need to develop methods capable of evaluating these processes. This is further motivated because there is little in the literature focused on the cooperative effects between the various modes. For example, it should be the case that coalescence may be accelerated by Ostwald ripening, and Ostwald ripening may be slowed by coalescence as a result of their respective concentration dependencies.<sup>22</sup> However, many studies only examine either coalescence<sup>28–30</sup> or Ostwald ripening.<sup>20,31,32</sup> Directly observing these processes in concert would complement this work so as to develop a more complete picture of the system dynamics as a whole. Along these lines, a recent study sought to elucidate the relationship between coalescence and temperature in emulsions on the microscale using microfluidic flow and optical microscopy with spatial resolution in the several 100s of nanometers, owing to the optical diffraction limit.<sup>33</sup> Further, once such fundamental processes are understood, it may also be possible to investigate more complex morphologies and interactions, such as nested or bicontinuous structures and predator-prey interdroplet behavior. 34-37

Here, we describe a characterization method for direct observation of emulsions that enables classification and quantification of demulsification mechanisms. Liquid phase transmission electron microscopy (LPTEM)<sup>38–44</sup> enables these observations at the nanoscale with high temporal resolution, leveraging advances in image capture technology.<sup>45,46</sup> For this initial study, we sought to investigate an emulsion that is relatively well understood by more conventional methods (*e.g.*, scattering,<sup>47–50</sup> and molecular dynamics and simulations<sup>51–53</sup>), but which is not conducive to traditional electron microscopy methods. Water-in-oil (w/o) emulsions are an ideal candidate for this, because they are common in the food and cosmetics industries but have a continuous organic phase which prevents them from being studied by dry state or cryogenic TEM without extensive optimization of sample preparation.<sup>24,54,55</sup> LPTEM, on the

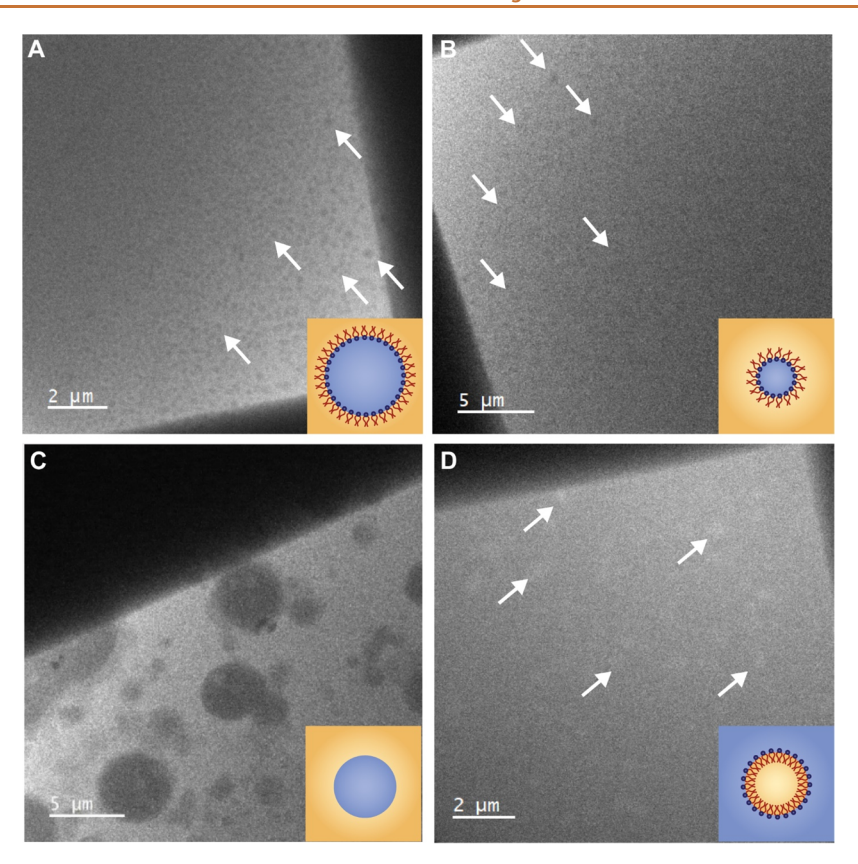


Figure 2. Initial emulsion formulations imaged by LPTEM, with schematic depictions in lower right. Images acquired at 0.1 e<sup>-</sup>/(Ų s) with Gatan OneView IS. (A) Water-in-isooctane emulsion at  $w_0 = 70$ . See also Supporting Information Video S1. (B) Water-in-isooctane emulsion at  $w_0 = 30$ . See also Video S2. (C) Water-in-isooctane emulsion without AOT stabilization. See also Video S4. (D) Isooctane-inwater emulsion at  $w_0 = 70$ . See also Video S5.

other hand, eschews the need to vitrify or dry these materials and avoids high-pressure freezing, while maintaining morphological integrity. The system of choice was the sodium salt of dioctyl sulfosuccinate (aerosol OT or AOT) with water and isooctane. This system is well characterized and may be made as either the oil-in-water or water-in-oil formulation by varying the relative quantities of each phase. Further, the system is well characterized such that our *in situ* findings can be corroborated with a substantial body of data. <sup>47,49,51,56–60</sup> In addition, this system is ideal in its modularity—the size of the initial micelles may be tuned by adjusting the surfactant loading ratio (i.e., the molar ratio of water to surfactant, referred to as  $w_0$ ). The emulsion was prepared via established protocols, dispersed via vortex mixing, and then kept in a sonication bath to maintain its morphological integrity prior to observation by LPTEM. 51,61,62 Critically, imaging by this method could be reproducibly achieved to capture morphology and, with rapid frame rates of videographic image capture, emulsion dynamics could be observed.63

#### **RESULTS AND DISCUSSION**

Prior to study via LPTEM, formulation of the emulsion was confirmed via dynamic light scattering to ensure that the population was in good agreement with the theoretically predicted size (~20 nm) (Supporting Information Figure S1). Dry state TEM was then attempted on the samples. However, due to the nature of the sample preparation (i.e., drying), no structures were detected, as anticipated. Next, the samples were loaded into a solution cell in preparation for LPTEM

(Figure S2). Surface chemistry optimization of the  $SiN_x$  chips revealed that avoiding the usual plasma cleaning step resulted in superior wetting of the sample across the surface—when the chips are made hydrophilic, the cell appeared largely dry, with some regions of phase separation visible (Figure S3). However, without plasma cleaning, the cells produced are clearly hydrated, with uniform and discrete droplets filling the cell (Figure 2). Hydration is evidenced by the intensity gradient across the cell, which is indicative of the characteristic bulging of the liquid.66 Upon initial irradiation, dispersed droplets are visible within the liquid cell (Figure 2A,B and Videos S1, S2, and S3). Prolonged beam exposure resulted in droplet growth, movement, and interaction (Video S1). These droplets were higher contrast against a lower contrast matrix and exhibited smooth and continuous motion. Qualitatively, this suggests that the droplets are completely solvated—because they do not adhere to the SiN<sub>x</sub> window, there is almost certainly a layer of the continuous phase between the droplet interface and the window. Typically, when in situ motion is analyzed, particles will move in jumps and will periodically "stick" and remain stationary between "slips" in motion<sup>67–70</sup>—this behavior was absent, suggesting that there are fewer interactions with the  $SiN_x$  interface. Subsequently, we were able to modulate the size of the initial droplets *via* surfactant loading ratio  $(w_0)$ —below, we show that by lowering  $w_0$  by a factor of  $\sim 2$ , we were able to reduce the size of the droplets at the time of initial irradiation (Figure 2A and Video S2 vs Figure 2B and Video S3).

Next, water was mechanically dispersed in isooctane without addition of surfactant. The results show that, despite following identical sample preparations, the observed droplets are far less

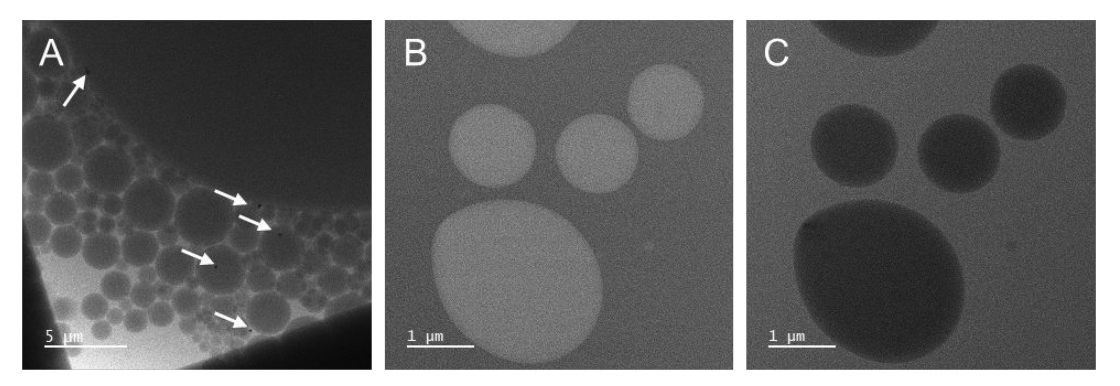


Figure 3. Phase determination of emulsified droplets. (A) Aqueous citrate-stabilized gold nanoparticles (indicated by white arrows) in isooctane stabilized by AOT, (B) ADF, and (C) BF STEM of water in isooctane stabilized by AOT.

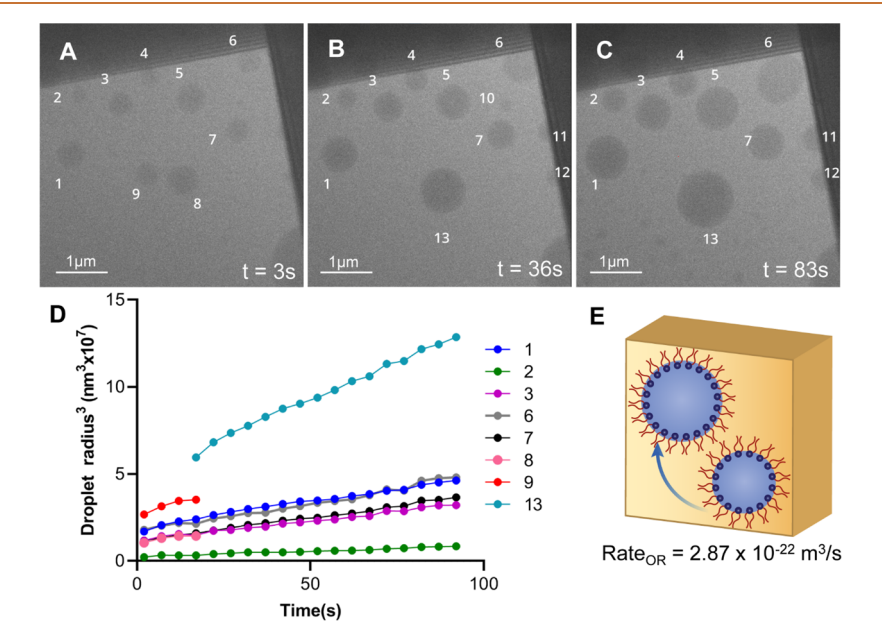


Figure 4. Quantification of Ostwald ripening of water droplets at low electron flux. (A, B, C) Observation of Ostwald ripening in water droplets at a flux of 0.19  $e/(A^2 s)$  and 12.5 FPS with Gatan OneView IS. Frames have been temporally binned 12 times for ease of observation. Droplets 8 and 9 merge at t = 15 s, and the resulting droplet is referred to as droplet 13. (D) Growth of selected droplets as  $r^3(t)$ , to evaluate rates of Ostwald ripening (slope of curves). Data sets are pruned to show selected droplets and are averaged every ten points. The full data set is given in Figure S6. (E) Schematic depiction of growth process and calculated Ostwald ripening rate.

uniform and often appear to have layered droplets, containing isooctane within the water droplets (Figure 2C). The aqueous domains have diffuse borders and are not well defined droplets, resulting from the lack of a surfactant-stabilized interface. When viewed in motion, the behavior of these droplets is distinctly different from those stabilized by the surfactant, with the water appearing to smear across and adhere to the  $\mathrm{SiN}_x$  windows (Video S4). The distinction between the two types of behaviors observed is an indication that the observation of well defined droplets is dependent on surfactant being present. Therefore, the sample may be safely imaged, maintaining surfactant integrity at electron fluxes of <1 e^-/(Ų s) and total fluence of 400 e^-/Ų.

Subsequently, we shifted the formulation to generate an oil-in-water (o/w) emulsion (Figure 2D). The o/w formulation at the same surfactant loading ratio yielded isooctane droplets that appeared roughly the same size as the initial water droplets from previous experiments. They are stable for longer under imaging conditions which may be attributed to the hindered transport of oil through water due to its larger molar volume

with respect to the reverse formulation. The isooctane droplets appear lower in contrast against the denser aqueous phase, which scatters electrons more strongly than in the reverse case. Thus, the droplets appear light against a dark background and are more difficult to resolve, but may still be seen to be moving freely (Video S5). This seemingly unhindered motion persisted for an extended period of imaging (several minutes at low flux) and qualitatively accelerated upon increasing beam strength, consistent with previous reports of beam-induced motion. 67,69,71 Capturing these dynamic events necessitates consideration of frame rates and image acquisition parameters. With a finite amount of signal, high frame rates give better temporal resolution but also reduces the signal acquired per frame, thus reducing spatial resolution. Conditions of electron flux, camera capture speed, and image resolution must be chosen judiciously (Figure S4).

We verified the identity of the phases first on the basis of solvent density, which should be directly proportional to its contrast, indicating that the dark droplets observed were the aqueous phase (as described above) for the water-in-oil

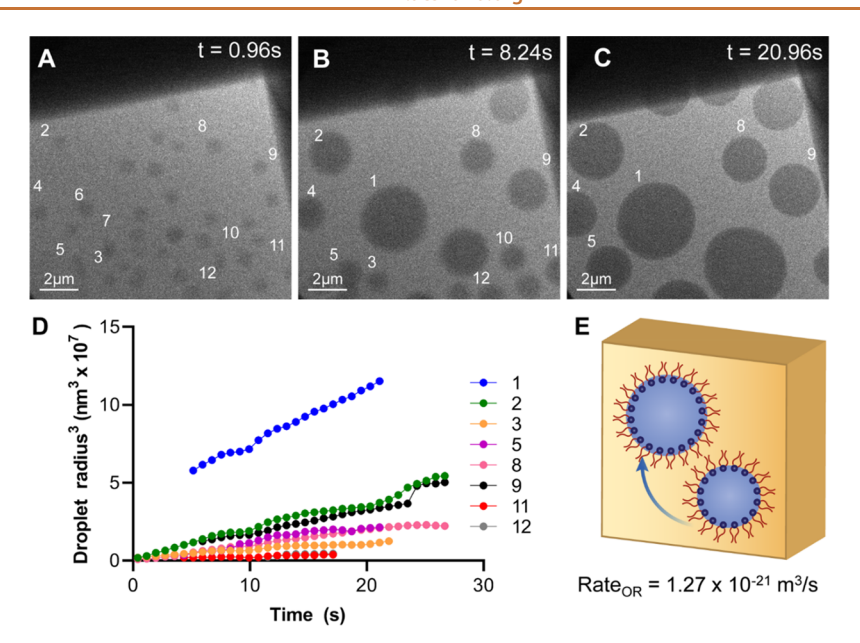


Figure 5. Observed Ostwald ripening at moderate electron flux. (A, B, C) Ostwald ripening of water in isooctane at a flux of  $0.5 \text{ e}^{-/(\text{Å}^2 \text{ s})}$  and 25 FPS with Gatan OneView IS at selected time steps from 0 to 30 s. (D) Growth of the radius cubed over time to quantify the rate of Ostwald ripening (slope of curves). Data sets are pruned to show selected droplets and are averaged every five points. The full data set is available in Figure S7. (E) Schematic depiction of Ostwald ripening and calculated Ostwald ripening rate.

emulsion, as intended (Figure 3).<sup>72</sup> However, to further corroborate this conclusion, citrate-stabilized aqueous gold nanoparticles were included in the aqueous phase (Figure 3A). These nanoparticles do not disperse in the oil phase and are of sufficient contrast to be easily distinguishable against either solvent. Upon imaging, the 100 nm Au particles were solely observed in the dark droplets, further verifying the assignment of phases. These observations were further supported by STEM imaging of the same formulation of the isooctane system (w/o,  $w_o = 70$ ). Annular dark field (ADF) images show the nucleated droplets lighter against a darker background, in contrast to the dark droplets seen in bright field imaging, indicating these droplets were of a higher density than the surrounding fluid (Figure 3B,C).

In addition, emulsions could be generated using decane and *n*-octane as the solvent and using formamide and dimethylformamide as dispersed phases following the same sample preparation procedure (Figure S5). This speaks to the versatility of LPTEM for imaging emulsions generally, without the need for optimized sample preparation that one would encounter for freeze-fracture and for high-pressure freezing. <sup>32,54</sup>

Qualitatively, we consistently observed all of the aforementioned modes of demulsification in the surfactant-stabilized experiments (Figure 1). However, it is necessary to be able to classify these processes and compare them to *ex situ* behavior and to understand differences based on formulation. In the case where droplet growth was observed, this was achieved by applying a simple image binarization algorithm to videos of stationary droplets which were observed to be increasing in size (Figures 4 and 5). After binarization, a function was applied to measure the area of each of the observed droplets; assuming a near-circular morphology, the resulting droplet diameter was then calculated. This process was iterated over subsequent frames to establish growth curves over time (Figure 4A–C and Video S6). For w/o formulations undergoing Ostwald ripening, it was anticipated that  $r^3$  would

be linear in time, which was the case (Figure 4D).  $^{24,25,28,73,74}$  Utilizing methods outlined by Jiao and Burgess,  $^{24}$  the estimated rate of Ostwald ripening for this formulation was  $6.034 \times 10^{-22}$  m<sup>3</sup>/s.

Initial observations at low electron flux (0.19 e/(Å2 s)), resulted in experimental Ostwald ripening rates on the expected order of magnitude (2.87  $\times$  10<sup>-22</sup> m<sup>3</sup>/s) (Figure 4E). Notably, in these images, we see that the diameters of the droplets are on the order of a few hundred nanometers, with the largest approaching micrometer scale. This exceeds the dimension of the liquid cell in the z-axis, and thus the droplets are assumed to be spheroidal, rather than true spheres. Accordingly, accumulated volume will disproportionately expand the droplet in the x-y plane, leading to a more rapid increase of radius than a sphere experiencing equivalent mass transport—this phenomenon would be expected to inflate calculated rates of Ostwald ripening. In contrast, these confined droplets are only able to receive mass through a fraction of their total surface area, unlike a true sphere. The magnitudes of these two deviations are approximately equal and opposite, such that we may continue to accurately model these ellipsoidal droplets as spheres (Figure S8). To briefly consider surface tension effects, one may consider that as the droplets are compressed, the curvature of the available surface area increases. This is an effective decrease in the radii of curvature, which would increase surface tension and, accordingly, the anticipated rate of Ostwald ripening. In that vein, one might expect that the most compressed droplets (i.e., those nearest the corner of the cell) should undergo the fastest growth. However, this is not the case, with the rates of Ostwald ripening not differing significantly as a function of location in the cell. Thus, we consider such effects negligible. An additional analysis of this is included in the Supporting Information.

Upon increasing electron flux, an increase in the rate of droplet growth was observed (Figure 5 and Video S7). An identical analysis to that previously described for the low-flux

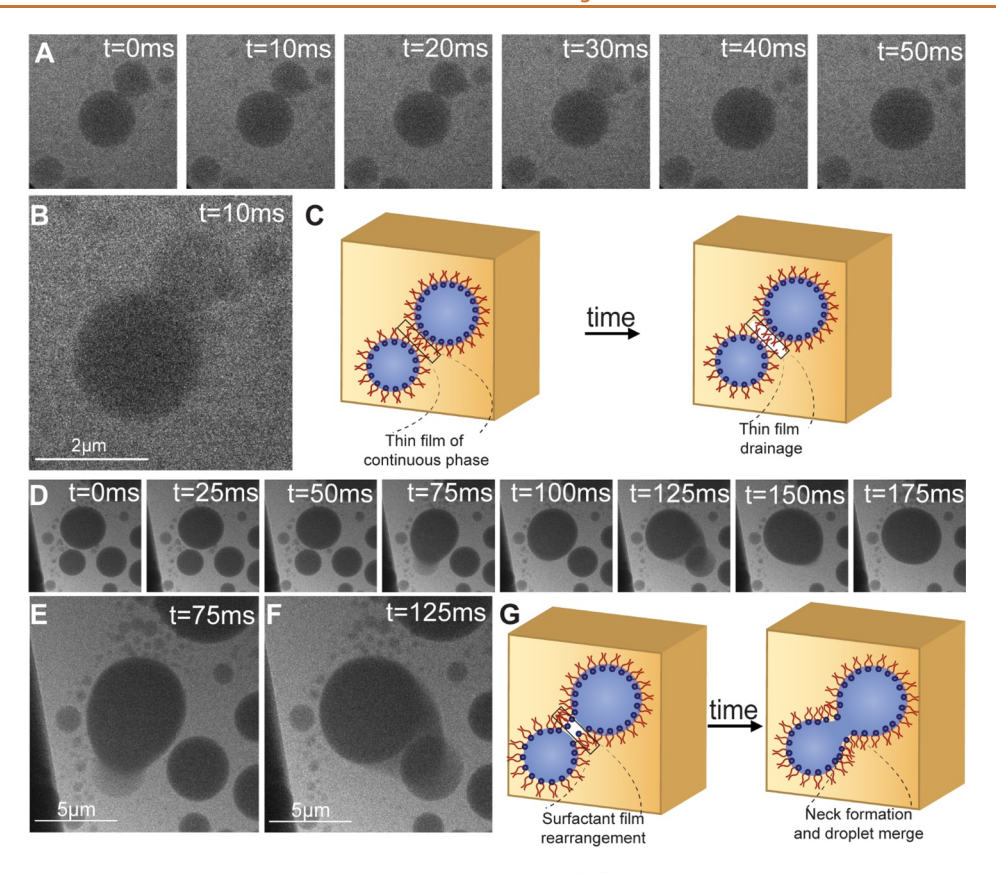


Figure 6. Observation of two distinct droplet coalescence intermediates. (A) Sequential frames before, during, and after first stage coalescence event. Each box measures 4.65  $\mu$ m square. (B) Intermediate dumbbell at t=30 ms, shown approximately 1.5× larger for detail. (C) Schematic representation of continuous phase thin film formation and drainage. (D) Observation of second droplet coalescence intermediate, with sequential frames before, during, and after two coalescence events at t=75 and 125 ms, shown approximately 2× larger in (E) and (F), respectively. Boxes here are 6.83  $\mu$ m square. (G) Schematic depiction of surfactant film rearrangement and droplet drainage. Images were captured at 100 FPS with Gatan OneView IS at a flux of 0.3  $e^-/(Å^2 s)$ .

Ostwald ripening data was followed, and the rates of Ostwald ripening were accordingly measured to be  $1.27 \times 10^{-21}$  m<sup>3</sup>/s (Figure 5D,E), an order of magnitude greater than that of the low-flux experiment, and thus an order of magnitude greater than expected. Being able to modulate dynamics by adjusting the electron beam is an indication that it may be possible to use this technique for characterizing accelerated aging. That is, understanding how these materials will behave over longer lifetimes at a shorter experimental time scale. For this system, Ostwald ripening rates may be approximated as a step function, wherein observed rates match expectation at low fluxes and accelerate once the threshold of safe imaging conditions are crossed, due to qualitative observations that droplet growth proceeded at a constant rate below a flux of 0.5 e/( $Å^2$  s). However, it may be the case that emulsions composed of other solvents and/or surfactants may be more sensitive to irradiation and may thus have a linear response to increased flux, even below the safe imaging threshold. In this case, it would be necessary to establish a calibration curve via variable dose experiments to accurately determine Ostwald ripening from such experiments.

Coalescence was observed across all emulsions containing surfactants. Notably, by increasing frame rates from those typically used for *in situ* microscopy (*e.g.*, 1–10 frames/s) to up to 100 frames/s, it was possible to observe merging events and to identify intermediates which have not previously been directly observed (Figure 6). In accordance with the models of coalescence, we were able to observe several intermediate

phases, consisting of both thin film drainage and subsequent rupture, wherein we were able to observe discrete merging events (Figure 6A–C, Video S8 and Figure 6D–G, Video S9, respectively).

The smaller droplet observed was in contact with the larger one for several seconds prior to merging, indicating that simply colliding with another droplet is not sufficient to initiate this process (Figure 6A). Rather, the continuous phase needs to dissipate such that the surfactant molecules are able to interact and rearrange (Figure 6B,C). This is referred to as thin film formation and drainage, wherein a small layer of isooctane remains between the two water droplets, attracted to the nonpolar portions of the AOT, and subsequent suction and disjoining pressure induced by electrostatic and van der Waals dispersion forces lead to its drainage (Figure 6B,C).75,76 Indeed, this thin film is visible in the videographic data, wherein a sliver of continuous phase may be seen between the two droplets in contact for an extended period (Video S8). This is consistent with the identification of thin film drainage as the rate limiting step in this process. Once the thin film of isooctane has dissipated, the surfactants are able to come into contact and rearrange, permitting the flow of water from one droplet into another (Figure 6D-G).75 This occurred twice during the acquisition of videographic data on this sample, observed at 40 frames/s (Video S9). In these intermediate frames, the flow of water from the smaller to the larger droplet can clearly be seen (Figure 6E,F). Information about such processes on the nanoscale can be utilized to glean information

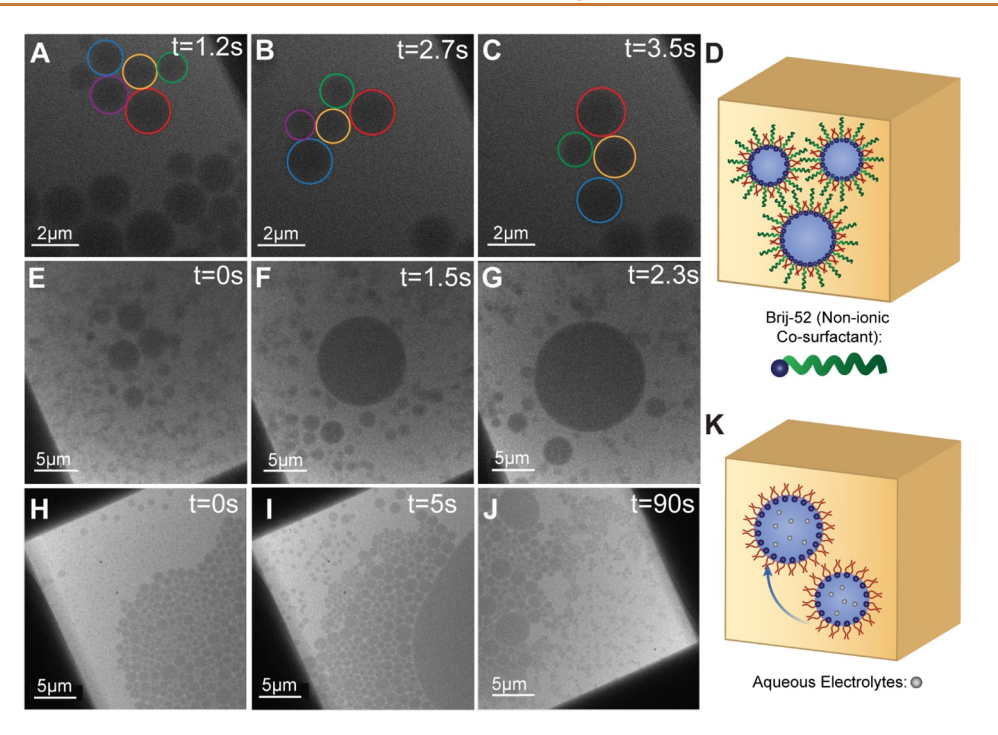


Figure 7. Shifting of observed demulsification modes via inclusion of specific additives. (A, B, C) Promotion of flocculation via addition of non-ionic cosurfactant. Colored circles are included as droplet identifiers. (D) Schematic depiction of droplets containing non-ionic surfactant (green lines) and how this relates to steric interactions. (E–G) Droplets only stabilized with AOT over a comparable time period for reference. (H, I, J) Morphology and growth of DPBS stabilized by AOT in isooctane over time. Notably, the population of very small droplets persists for significantly longer time scales due to electrolyte-inhibited Ostwald ripening. (K) Schematic depiction of slowed Ostwald ripening, with electrolytes denoted by gray spheres. Images were acquired with the Gatan OneView IS at a flux of  $0.3 \, \mathrm{e}^-/(\mathrm{Å}^2 \, \mathrm{s})$  at 10 FPS.

regarding the energetics of such interactions and the surface tension of the droplets involved.

Given our observation of demulsification for a given formulation (water in isooctane,  $w_0 = 70$ ), the next step was to see if that degradation could be altered via known strategies-namely, the inclusion of a cosurfactant or additional solute components (Figure 7). These additives are known to inhibit coalescence and Ostwald ripening, respectively, due to increased steric hindrance of the droplets and equalized Laplace pressure. 77-80 If these shifts were observed in situ, it would further confirm that the behaviors are reflective of bulk solution behavior. For cosurfactant, BRIJ-52, a non-ionic poly(ethylene glycol)-based surfactant, was selected due to its ability to increase the solubilization capacity of water.<sup>58</sup> This was mixed with AOT in equimolar quantities, such that the overall surfactant-to-water ratio remained consistent with previous experiments ( $w_0 = 70$ ). This formulation showed a propensity for flocculation prior to coalescence, as a result of the steric hindrance introduced by BRIJ-52. Droplets were consistently observed to collide and adhere for a greater time scale (several seconds) prior to coalescence than in comparable formulations without the inclusion of BRIJ-52 (such as those previously discussed with Figure 6) (Figure 7A–G, Video S10).

To modulate Ostwald ripening, electrolytes were chosen as solutes, due to their incompatibility with isooctane and other alkanes. Hence, water was replaced with Dulbecco's phosphate buffered saline (DPBS). In this scenario, the observed population of small (sub-300 nm) droplets was significantly larger than previously seen and the lifetime of these droplets was significantly prolonged, as evidenced by

their presence over several minutes of imaging (Figure 7H–J, Video S11). Further, a foam-like morphology was observed upon initial irradiation, showing increased droplet stability to flocculation (Figure 7H,I). While this was unanticipated, it is possible that this may have been the result of Coulombic interactions introduced by the saline, leading to increased hindrance to coalescence. Competing forces of adhesion and compression are also at play, which may contribute to the foam morphology seen. The appearance and duration of such a foam-like structure were not seen with any of the other variations studied. The introduction of increased electrostatic interactions may also contribute to repulsive forces between the droplets, leading to increased stability upon adhesion. Further, when used in conjunction with an ionic surfactant such as AOT, the included electrolytes will contribute to charge screening effects, which can further increase stabilization and affect emulsion morphology.81,82

As with all *in situ* experiments, the effect of electron beam irradiation must be considered. While we are able to mitigate some of this effect by using minimal fluxes and fluences, interactions between the high-energy incident electrons and the sample still remain. Copious qualitative evidence demonstrates the acceleration of demulsification upon increasing flux, and the measured rate of Ostwald ripening confirms this. On thus, despite efforts to lessen the beam's confounding influence, it must still be considered. High-flux experiments demonstrated that, beyond a certain fluence (400 e<sup>-</sup>/Å<sup>2</sup>), the observed phases of water-in-isooctane emulsions will reverse. That is, the water becomes the continuous phase within the imaging region and droplets of lighter isooctane are observed (Figure S9). This behavior is consistent across

multiple high-fluence experiments (both high-flux and extended imaging conditions). In such cases, beam blanking will permit the return of the oil phase to the cell; however, the oil-in-water emulsion quickly flows in from the corner (Video S12). We hypothesize that this preferential interaction between the water and the beam is the result of charging imposed upon the SiN<sub>x</sub> by the electron beam. Thus, this compositional shift seems to be irreversible and may result from either damage to the surfactant or heightened local concentrations of water such that the original formulation is no longer thermodynamically favorable. We posit that such drastic changes in phase distribution within the cell may be an interesting strategy to induce mixing or changes in phase behavior during in situ experiments. Additionally, during STEM experiments, droplets nucleated with a teardrop morphology, with the point forming at the upper left and the bulb forming at the lower right (Figure 3B,C). This orientation is consistent with the raster pattern of the electron probe, indicating that the impinging electrons are affecting the nucleation and growth. These mechanisms and transformations are not yet understood and are an intriguing area for further study. However, our collective observations and characterizations indicate to us that, at low fluxes and fluences, the beam serves to accelerate the observed processes.

## **CONCLUSIONS**

Using low electron flux LPTEM imaging, we have observed the unperturbed morphology of emulsions in the solution phase. This is difficult or impossible by other methods. Further, LPTEM allows for the observation of emulsion evolution over time. We have been able to directly monitor the way these processes change as a result of formulation modifications and subsequently confirm these changes *via* image analysis. Further, the observed changes in the emulsion behavior from additives are consistent with bulk trends, making this an effective way of investigating surfactant—solute interactions. In summary, this methodology is a relatively simple and streamlined way of evaluating emulsions. The implementation of such a method may accelerate emulsion and surfactant development, as well as lead to further insight into the mechanisms of formation and demulsification.

## **METHODS**

**Emulsion Preparation.** AOT was dissolved in isooctane at the desired molar concentration, after which deionized Milli-Q water was added to achieve the proper surfactant loading ratio ( $w_o$ ). The dispersion was then vortexed for 2 min to mechanically disperse the droplets and was subsequently stabilized in a sonication bath until studied. For the reverse phase emulsion (o/w), the AOT was first dissolved in water, with isooctane subsequently added and dispersed as above. For all other included components (buffer, salts, and alternate solvents), the same protocol was followed.

**Dynamic Light Scattering Analysis.** Dynamic light scattering was used to determine the size of the emulsion droplets with a Wyatt DynaPro NanoStar.

**Liquid Phase Transmission Electron Microscopy.** LPTEM experiments were performed using Hummingbird Scientific Dual Flow Mixing and Protochips Poseidon Select holder. In both cases, the cell preparation was as follows: the lines were left unfilled with solvent.  $SiN_x$  chips for the respective holders were not plasma cleaned for solutions with a nonpolar dispersed phase, or plasma cleaned for 30 s for aqueous samples. Samples of 0.8  $\mu$ L aliquots each were deposited onto the bottom chip via micropipette. Top chips were placed to ensure orthogonal alignment of the windows (creating a 50  $\mu$ m by 50  $\mu$ m viewing area) and were manually aligned before sealing

with the holders' appropriate hardware (lid for Protochips, top clamp for Hummingbird). Assembled cells were vacuum tested in an external pumping station to ensure liquid cell integrity at relevant pressures  $(8.6 \times 10^{-6} \text{ mbar})$  prior to insertion in the microscope. A JEM-ARM300F (JEOL Ltd., Tokyo, Japan) transmission electron microscope was used for in situ experiments at an operating voltage of at 300 keV and current of 15  $\mu$ A (FEG source). Images were acquired with a Gatan  $2k \times 2k$  OneView IS CMOScamera and a Gatan K3-IS direct electron detector (Gatan Inc., Pleasanton, CA, USA) via Gatan Digital Micrograph imaging software (Roper Technologies, Sarasota, FL, USA). Exposure durations ranged from 0.01 to 1 s. Electron fluxes were measured both by the K3 and via the detected beam current, which has previously been calibrated via a Faraday holder in conjunction with the respective apertures used. Video acquisition was done by either the in situ camera functionalities or by screen recording with Camtasia Studio 2018 (TechSmithCorporation, USA). Frame rates for each data set are as indicated in figure captions. STEM images were acquired under the same operating conditions, using a probe size of 8C, camera length of 40 cm, and a 40  $\mu m$ aperture, with a pixel dwell time of 2.4 µs. Images were collected with bright field and annular dark field detectors as indicated.

#### **ASSOCIATED CONTENT**

# Supporting Information

The Supporting Information is available free of charge at https://pubs.acs.org/doi/10.1021/acsnano.2c00199.

Video S1 showing LPTEM data of isooctane/AOT/ water at  $w_o = 70$  acquired with an electron flux of 0.078  $e^-/(\mathring{A}^2 s)$  (AVI)

Video S2 showing LPTEM data of isooctane/AOT/ water at  $w_o = 30$  acquired with an electron flux of 0.078  $e^-/(\mathring{A}^2 s)$  (AVI)

Video S3 showing LPTEM data of droplet growth and behavior (AVI)

Video S4 showing LPTEM data of mechanically dispersed water in isooctane acquired with an electron flux of 0.19  $e^-/(\mathring{A}^2 s)$  (AVI)

Video S5 showing LPTEM data of water/AOT/ isooctane at  $w_0 = 70$  acquired with an electron flux of 1.0 e<sup>-</sup>/(Å<sup>2</sup> s) (AVI)

Video S6 showing LPTEM data of water droplets undergoing Ostwald ripening in isooctane, acquired with an electron flux of  $0.19 \text{ e}^{-}/(\text{Å}^2 \text{ s})$  (AVI)

Video S7 showing LPTEM data of water droplets undergoing Ostwald ripening in isooctane, acquired with an electron flux of 0.5 e $^-$ /(Å $^2$  s) (AVI)

Video S8 showing LPTEM data of water droplets coalescing with a visible thin film formation, acquired with an electron flux of  $0.3~e^-/(\mbox{Å}^2~s)$  (AVI)

Video S9 showing LPTEM data of water droplets coalescing with a visible thin film drainage, acquired with an electron flux of  $0.3 \text{ e}^-/(\text{Å}^2 \text{ s})$  (AVI)

Video S10 showing LPTEM data of water droplets flocculating as a result of the inclusion of a non-ionic cosurfactant (Brij-52), acquired with an electron flux of 0.1  $e^-/(\mathring{A}^2~s)$  (AVI)

Video S11 showing LPTEM data of slowed Ostwald ripening of water droplets as a result of the inclusion of electrolytes, acquired with an electron flux of 0.1  $e^-/(\mathring{A}^2~s)~(\mathrm{AVI})$ 

Video S12 showing LPTEM data of reversed-phase emulsion behavior at high cumulative fluence ( $\sim$ 500 e/ Å<sup>2</sup>) (AVI)

Figures of liquid cell assembly, DLS measurements, liquid phase and dry state TEM images, supplemental

data and analysis of Ostwald ripening rates, and discussion of image processing (PDF)

# **AUTHOR INFORMATION**

#### **Corresponding Author**

Nathan C. Gianneschi — Department of Materials Science & Engineering, Northwestern University, Evanston, Illinois 60208, United States; International Institute for Nanotechnology, Simpson Querrey Institute, Chemistry of Life Processes Institute and Department of Chemistry, Department of Biomedical Engineering, Department of Pharmacology, Northwestern University, Evanston, Illinois 60208, United States; orcid.org/0000-0001-9945-5475; Email: Nathan.gianneschi@northwestern.edu

#### **Author**

Maria A. Vratsanos — Department of Materials Science & Engineering, Northwestern University, Evanston, Illinois 60208, United States; orcid.org/0000-0001-8377-4113

Complete contact information is available at: https://pubs.acs.org/10.1021/acsnano.2c00199

#### Notes

The authors declare no competing financial interest.

#### **ACKNOWLEDGMENTS**

We acknowledge support of this work through government funding awarded through the Army Research Office (Grants W911NF-17-1-0326, W911NF-18-1-0359, and MURI W911NF-15-1-0568) and the National Science Foundation (Grant CHE-MSN 1905270). This work made use of the EPIC facility within Northwestern University's NUANCE facility, which receives support from the Soft and Hybrid Nanotechnology Experimental (SHyNE) Resource (Grant NSF ECCS-202563), the International Institute for Nanomaterials (Grant NIH-S10OD026871), and the Materials Research Science and Engineering Centers (Grant NSF DMR-1720139). Research reported in this publication was supported in part by instrumentation provided by the Office of The Director of the National Institutes of Health under Award No. S10OD026871. The content is solely the responsibility of the authors and does not necessarily represent the official views of the National Institutes of Health. M.A.V. is grateful for the support of the National Science Foundation through their Graduate Research Fellowship (Grant DGE-1842165) and of Northwestern University via the Dr. John N. Nicholson Fellowship. Proctor & Gamble also generously contributed to this study via a gift to Northwestern University. We are grateful to Karthikeyan Gnanasekaran for fruitful discussions.

# **REFERENCES**

- (1) Gupta, A.; Eral, H. B.; Hatton, T. A.; Doyle, P. S. Nanoemulsions: Formation, Properties and Applications. *Soft Matter* **2016**, *12* (11), 2826–2841.
- (2) Mason, T. G.; Wilking, J. N.; Meleson, K.; Chang, C. B.; Graves, S. M. Nanoemulsions: Formation, Structure, and Physical Properties. *J. Phys.: Condens. Matter* **2006**, *18* (41), R635–R666.
- (3) Griffin, W. C. Calculation of HLB Values of Non-Ionic Surfactants. *J. Soc. Cosmet. Chem.* **1954**, *5* (4), 249–256.
- (4) Griffin, W. C. Classification of Surface-Active Agents by "HLB". *J. Soc. Cosmet. Chem.* **1949**, *1* (5), 311–326.

- (5) Surfactants in Consumer Products: Theory, Technology, and Application; Falbe, J., Ed.; Springer: Berlin, Heidelberg, 1987. DOI: 10.1007/978-3-642-71545-7.
- (6) McClements, D. J. Critical Review of Techniques and Methodologies for Characterization of Emulsion Stability. *Crit. Rev. Food Sci. Nutr.* **2007**, 47 (7), 611–649.
- (7) Zhu, Q.; Pan, Y.; Jia, X.; Li, J.; Zhang, M.; Yin, L. Review on the Stability Mechanism and Application of Water-in-Oil Emulsions Encapsulating Various Additives. *Comprehensive Reviews in Food Science and Food Safety* **2019**, *18* (6), 1660–1675.
- (8) McClements, D. J.; Jafari, S. M. Improving Emulsion Formation, Stability and Performance Using Mixed Emulsifiers: A Review. *Adv. Colloid Interface Sci.* **2018**, 251, 55–79.
- (9) Weiss, J.; Herrmann, N.; McClements, D. J. Ostwald Ripening of Hydrocarbon Emulsion Droplets in Surfactant Solutions. *Langmuir* 1999, 15 (20), 6652–6657.
- (10) Tadros, T.; Izquierdo, P.; Esquena, J.; Solans, C. Formation and Stability of Nano-Emulsions. *Adv. Colloid Interface Sci.* **2004**, 108–109, 303–318
- (11) Czajka, A.; Armes, S. P. Time-Resolved Small-Angle X-Ray Scattering Studies during Aqueous Emulsion Polymerization. *J. Am. Chem. Soc.* **2021**, *143* (3), 1474–1484.
- (12) Santos, J.; Calero, N.; Trujillo-Cayado, L. A.; Garcia, M. C.; Muñoz, J. Assessing Differences between Ostwald Ripening and Coalescence by Rheology, Laser Diffraction and Multiple Light Scattering. *Colloids Surf.*, B **2017**, 159, 405–411.
- (13) Narayan, S.; Metaxas, A. E.; Bachnak, R.; Neumiller, T.; Dutcher, C. S. Zooming in on the Role of Surfactants in Droplet Coalescence at the Macroscale and Microscale. *Curr. Opin. Colloid Interface Sci.* **2020**, *50*, 101385.
- (14) Sommerling, J. H.; de Matos, M. B. C.; Hildebrandt, E.; Dessy, A.; Kok, R. J.; Nirschl, H.; Leneweit, G. Instability Mechanisms of Water-in-Oil Nanoemulsions with Phospholipids: Temporal and Morphological Structures. *Langmuir* **2018**, *34* (2), 572–584.
- (15) Nazarzadeh, E.; Anthonypillai, T.; Sajjadi, S. On the Growth Mechanisms of Nanoemulsions. *J. Colloid Interface Sci.* **2013**, 397, 154–162.
- (16) Rodriguez-Lopez, G.; O'Neil Williams, Y.; Toro-Mendoza, J. Individual and Collective Behavior of Emulsion Droplets Undergoing Ostwald Ripening. *Langmuir* **2019**, *35* (15), 5316–5323.
- (17) Wooster, T. J.; Golding, M.; Sanguansri, P. Impact of Oil Type on Nanoemulsion Formation and Ostwald Ripening Stability. *Langmuir* **2008**, 24 (22), 12758–12765.
- (18) Kabal'nov, A. S.; Pertzov, A. V.; Shchukin, E. D. Ostwald Ripening in Two-Component Disperse Phase Systems: Application to Emulsion Stability. *Colloids Surf.* **1987**, *24* (1), 19–32.
- (19) Hunter, S. J.; Cornel, E. J.; Mykhaylyk, O. O.; Armes, S. P. Effect of Salt on the Formation and Stability of Water-in-Oil Pickering Nanoemulsions Stabilized by Diblock Copolymer Nanoparticles. *Langmuir* **2020**, *36* (51), 15523–15535.
- (20) Taylor, P. Ostwald Ripening in Emulsions. *Adv. Colloid Interface Sci.* 1998, 75 (2), 107–163.
- (21) Santos, J.; Calero, N.; Trujillo-Cayado, L. A.; Garcia, M. C.; Muñoz, J. Assessing Differences between Ostwald Ripening and Coalescence by Rheology, Laser Diffraction and Multiple Light Scattering. *Colloids Surf.*, B **2017**, 159, 405–411.
- (22) Schmitt, V.; Leal-Calderon, F. Measurement of the Coalescence Frequency in Surfactant-Stabilized Concentrated Emulsions. *Europhys. Lett.* **2004**, *67* (4), 662–668.
- (23) Nazarzadeh, E.; Anthonypillai, T.; Sajjadi, S. On the Growth Mechanisms of Nanoemulsions. *J. Colloid Interface Sci.* **2013**, 397, 154–162.
- (24) Jiao, J.; Burgess, D. J. Ostwald Ripening of Water-in-Hydrocarbon Emulsions. *J. Colloid Interface Sci.* **2003**, 264 (2), 509–516.
- (25) Koroleva, M. Yu; Yurtov, E. V. Ostwald Ripening in Macro- and Nanoemulsions. *Russ. Chem. Rev.* **2021**, *90* (3), 293–323.

- (26) Rodriguez-Lopez, G.; O'Neil Williams, Y.; Toro-Mendoza, J. Individual and Collective Behavior of Emulsion Droplets Undergoing Ostwald Ripening. *Langmuir* **2019**, *35* (15), 5316–5323.
- (27) Hassan, P. A.; Rana, S.; Verma, G. Making Sense of Brownian Motion: Colloid Characterization by Dynamic Light Scattering. *Langmuir* **2015**, *31* (1), 3–12.
- (28) Urbina-Villalba, G.; Forgiarini, A.; Rahn, K.; Lozsan, A. Influence of Flocculation and Coalescence on the Evolution of the Average Radius of an O/W Emulsion. Is a Linear Slope of  $\overline{R}^3$  vs. t an Unmistakable Signature of Ostwald Ripening ? *Phys. Chem. Chem. Phys.* **2009**, 11 (47), 11184–11195.
- (29) Wang, H.; Davis, R. H. Droplet Growth Due to Brownian, Gravitational, or Thermocapillary Motion and Coalescence in Dilute Dispersions. *J. Colloid Interface Sci.* **1993**, 159 (1), 108–118.
- (30) Rekvig, L.; Frenkel, D. Molecular Simulations of Droplet Coalescence in Oil/Water/Surfactant Systems. *J. Chem. Phys.* **2007**, 127 (13), 134701.
- (31) Taylor, P. Ostwald Ripening in Emulsions: Estimation of Solution Thermodynamics of the Disperse Phase. *Adv. Colloid Interface Sci.* **2003**, *106* (1–3), 261–285.
- (32) Koroleva, M. Y.; Yurtov, E. V. Water Transport by Nanodispersion Droplets in a Water-in-Oil Emulsion. *Colloid Journal of the Russian Academy of Sciences: Kolloidnyi Zhurnal* **2003**, 65 (1), 35–39.
- (33) Bera, B.; Khazal, R.; Schroën, K. Coalescence Dynamics in Oilin-Water Emulsions at Elevated Temperatures. *Sci. Rep.* **2021**, *11* (1), 1–10
- (34) Meredith, C. H.; Moerman, P. G.; Groenewold, J.; Chiu, Y.-J.; Kegel, W. K.; van Blaaderen, A.; Zarzar, L. D. Predator-Prey Interactions between Droplets Driven by Non-Reciprocal Oil Exchange. *Nature Chemistry* 2020 12:12 2020, 12 (12), 1136–1142.
- (35) Meredith, C. H.; Castonguay, A. C.; Chiu, Y.-J.; Brooks, A. M.; Moerman, P. G.; Torab, P.; Wong, P. K.; Sen, A.; Velegol, D.; Zarzar, L. D. Chemical Design of Self-Propelled Janus Droplets. *Matter* **2022**, 5 (2), 616–633.
- (36) Chen, S. H.; Chang, S. L.; Strey, R.; Samseth, J.; Mortensen, K. Structural Evolution of Bicontinuous Microemulsions. *J. Phys. Chem.* **1991**, 95 (19), 7427–7432.
- (37) Sheth, T.; Seshadri, S.; Prileszky, T.; Helgeson, M. E. Multiple Nanoemulsions. *Nat. Rev. Mater.* **2020**, *5*, 214–228.
- (38) de Jonge, N.; Ross, F. M. Electron Microscopy of Specimens in Liquid. *Nat. Nanotechnol.* **2011**, *6*, 695–704.
- (39) Evans, J. E.; Jungjohann, K. L.; Browning, N. D.; Arslan, I. Controlled Growth of Nanoparticles from Solution with in Situ Liquid Transmission Electron Microscopy. *Nano Lett.* **2011**, *11* (7), 2809–2813.
- (40) Abellan, P.; Woehl, T. J. Liquid Cell Electron Microscopy for the Study of Growth Dynamics of Nanomaterials and Structure of Soft Matter. In *In-situ Characterization Techniques for Nanomaterials*; Springer-Verlag: Berlin, Heidelberg, 2018; pp 1–31. DOI: 10.1007/978-3-662-56322-9 1.
- (41) Patterson, J. P.; Abellan, P.; Denny, M. S.; Park, C.; Browning, N. D.; Cohen, S. M.; Evans, J. E.; Gianneschi, N. C. Observing the Growth of Metal-Organic Frameworks by in Situ Liquid Cell Transmission Electron Microscopy. *J. Am. Chem. Soc.* **2015**, *137* (23), 7322–7328.
- (42) Gilmore, B. L.; Showalter, S. P.; Dukes, M. J.; Tanner, J. R.; Demmert, A. C.; McDonald, S. M.; Kelly, D. F. Visualizing Viral Assemblies in a Nanoscale Biosphere. *Lab Chip* **2013**, *13* (2), 216–219.
- (43) Mirsaidov, U. M.; Zheng, H.; Casana, Y.; Matsudaira, P. Imaging Protein Structure in Water at 2.7 Nm Resolution by Transmission Electron Microscopy. *Biophys. J.* **2012**, *102* (4), L15–L17
- (44) Woehl, T. J.; Evans, J. E.; Arslan, I.; Ristenpart, W. D.; Browning, N. D. Direct in Situ Determination of the Mechanisms Controlling Nanoparticle Nucleation and Growth. *ACS Nano* **2012**, *6* (10), 8599–8610.

- (45) McMullan, G.; Faruqi, A. R.; Henderson, R. Direct Electron Detectors. *In Methods in Enzymology* **2016**, *579*, 1–17.
- (46) Gatan. OneView Camera Model 1095 Datasheet, 2019; pp 4-7.
- (47) Fletcher, P. D. I.; Parrott, D. Water Droplet Coalescence Rates in Water-in-Oil Microemulsions. In *Reactions in Compartmentalized Liquids*; Springer: Berlin, Heidelberg, 1989; pp 53–60. DOI: 10.1007/978-3-642-74787-8 6.
- (48) Bergenholtz, J.; Romagnoli, A. A.; Wagner, N. J. Viscosity, Microstructure, and Interparticle Potential of AOT/H2O/n-Decane Inverse Microemulsions. *Langmuir* 1995, 11 (5), 1559–1570.
- (49) Nave, S.; Eastoe, J.; Penfold, J. What Is so Special about Aerosol-OT? 1. Aqueous Systems. *Langmuir* **2000**, *16* (23), 8733–8740.
- (50) Aferni, A. el; Guettari, M.; Tajouri, T. Determination of the Water/AOT/Isooctane Reverse Micelles Size Parameters from Their Refractive Index Data. *J. Solution Chem.* **2017**, *46* (1), 89–102.
- (51) Eskici, G.; Axelsen, P. H. The Size of AOT Reverse Micelles. *J. Phys. Chem. B* **2016**, *120* (44), 11337–11347.
- (52) Hensel, J. K.; Carpenter, A. P.; Ciszewski, R. K.; Schabes, B. K.; Kittredge, C. T.; Moore, F. G.; Richmond, G. L. Molecular Characterization of Water and Surfactant AOT at Nanoemulsion Surfaces. *Proc. Natl. Acad. Sci. U. S. A.* **2017**, *114* (51), 13351–13356.
- (53) Abel, S.; Sterpone, F.; Bandyopadhyay, S.; Marchi, M. Molecular Modeling and Simulations of AOT-Water Reverse Micelles in Isooctane: Structural and Dynamic Properties. *J. Phys. Chem. B* **2004**, *108* (50), 19458–19466.
- (54) Marchand, K. E.; Tarret, M.; Lechaire, J. P.; Normand, L.; Kasztelan, S.; Cseri, T. Investigation of AOT-Based Microemulsions for the Controlled Synthesis of MoSx Nanoparticles: An Electron Microscopy Study. *Colloids Surf., A* **2003**, 214 (1–3), 239–248.
- (55) Leung, R.; Shah, D. O. Solubilization and Phase Equilibria of Water-in-Oil Microemulsions. I. Effects of Spontaneous Curvature and Elasticity of Interfacial Films. *J. Colloid Interface Sci.* **1987**, *120* (2), 320–329.
- (56) Frank, S. G.; Zografi, G. Solubilization of Water by Dialkyl Sodium Sulfosuccinates in Hydrocarbon Solutions. *J. Colloid Interface Sci.* **1969**, 29 (1), 27–35.
- (57) Zulauf, M.; Eicke, H. F. Inverted Micelles and Microemulsions in the Ternary System Water/Aerosol-OT/Isooctane as Studied by Photon Correlation Spectroscopy. *J. Phys. Chem.* **1979**, 83 (4), 480–486.
- (58) Chatterjee, S.; Mitra, R. K.; Paul, B. K.; Bhattacharya, S. C. Interface of AOT/Brij Mixed Reverse Micellar Systems: Conductometric and Spectrophotometric Investigations. *J. Colloid Interface Sci.* **2006**, 298 (2), 935–941.
- (59) Yesibolati, M. N.; Mortensen, K. I.; Sun, H.; Brostrøm, A.; Tidemand-Lichtenberg, S.; Mølhave, K. Unhindered Brownian Motion of Individual Nanoparticles in Liquid-Phase Scanning Transmission Electron Microscopy. *Nano Lett.* **2020**, *20* (10), 7108–7115.
- (60) Parent, L. R.; Bakalis, E.; Proetto, M.; Li, Y.; Park, C.; Zerbetto, F.; Gianneschi, N. C. Tackling the Challenges of Dynamic Experiments Using Liquid-Cell Transmission Electron Microscopy. *Acc. Chem. Res.* **2018**, *51* (1), 3–11.
- (61) Wang, C.; Chen, X.; Wu, Y.; Li, Y.; Cheng, S. In Situ Liquid Cell Transmission Electron Microscopy Observation of Dynamic Process of Oleic Acid Emulsion with Gold Nanorods. *J. Phys. Chem. C* **2020**, *124* (47), 26018–26025.
- (62) Stawski, T. M.; Roncal-Herrero, T.; Fernandez-Martinez, A.; Matamoros-Veloza, A.; Kroger, R.; Benning, L. G. On Demand" Triggered Crystallization of CaCO3 from Solute Precursor Species Stabilized by the Water-in-Oil Microemulsion. *Phys. Chem. Chem. Phys.* **2018**, 20 (20), 13825–13835.
- (63) Korpanty, J.; Parent, L. R.; Gianneschi, N. C. Enhancing and Mitigating Radiolytic Damage to Soft Matter in Aqueous Phase Liquid-Cell Transmission Electron Microscopy in the Presence of Gold Nanoparticle Sensitizers or Isopropanol Scavengers. *Nano Lett.* **2021**, *21*, 1141–1149.

- (64) Park, J.; Park, H.; Ercius, P.; Pegoraro, A. F.; Xu, C.; Kim, J. W.; Han, S. H.; Weitz, D. A. Direct Observation of Wet Biological Samples by Graphene Liquid Cell Transmission Electron Microscopy. *Nano Lett.* **2015**, *15* (7), 4737–4744.
- (65) Wang, H.; Nagamanasa, K. H.; Kim, Y.-J.; Kwon, O.-H.; Granick, S. Longer-Lasting Electron-Based Microscopy of Single Molecules in Aqueous Medium. *ACS Nano* **2018**, *12* (8), 8572–8578.
- (66) Wu, H.; Su, H.; Joosten, R. R. M.; Keizer, A. D. A.; Hazendonk, L. S.; Wirix, M. J. M.; Patterson, J. P.; Laven, J.; With, G.; Friedrich, H. Mapping and Controlling Liquid Layer Thickness in Liquid-Phase (Scanning) Transmission Electron Microscopy. *Small Methods* **2021**, 5 (6), 2001287.
- (67) Bakalis, E.; Parent, L. R.; Vratsanos, M.; Park, C.; Gianneschi, N. C.; Zerbetto, F. Complex Nanoparticle Diffusional Motion in Liquid-Cell Transmission Electron Microscopy. *J. Phys. Chem. C* **2020**, *124* (27), 14881–14890.
- (68) Parent, L. R.; Bakalis, E.; Ramírez-Hernández, A.; Kammeyer, J. K.; Park, C.; de Pablo, J.; Zerbetto, F.; Patterson, J. P.; Gianneschi, N. C. Directly Observing Micelle Fusion and Growth in Solution by Liquid-Cell Transmission Electron Microscopy. *J. Am. Chem. Soc.* **2017**, 139 (47), 17140–17151.
- (69) Jamali, V.; Hargus, C.; Ben-Moshe, A.; Aghazadeh, A.; Ha, H. D.; Mandadapu, K. K.; Alivisatos, A. P. Anomalous Nanoparticle Surface Diffusion in LCTEM Is Revealed by Deep Learning-Assisted Analysis. *Proc. Natl. Acad. Sci. U. S. A.* **2021**, *118* (10), e2017616118.
- (70) Verch, A.; Pfaff, M.; de Jonge, N. Exceptionally Slow Movement of Gold Nanoparticles at a Solid/Liquid Interface Investigated by Scanning Transmission Electron Microscopy. *Langmuir* **2015**, *31* (25), 6956–6964.
- (71) Parent, L. R.; Bakalis, E.; Ramírez-Hernández, A.; Kammeyer, J. K.; Park, C.; de Pablo, J.; Zerbetto, F.; Patterson, J. P.; Gianneschi, N. C. Directly Observing Micelle Fusion and Growth in Solution by Liquid-Cell Transmission Electron Microscopy. *J. Am. Chem. Soc.* **2017**, 139 (47), 17140–17151.
- (72) Gnanasekaran, K.; Korpanty, J.; Berger, O.; Hampu, N.; Halperin-Sternfeld, M.; Cohen-Gerassi, D.; Adler-Abramovich, L.; Gianneschi, N. C. Dipeptide Nanostructure Assembly and Dynamics via in Situ Liquid-Phase Electron Microscopy. *ACS Nano* **2021**, *15*, 16542–16551.
- (73) Koroleva, M. Y.; Yurtov, E. V. Water Mass Transfer in W/O Emulsions. J. Colloid Interface Sci. 2006, 297 (2), 778–784.
- (74) Voorhees, P. W. The Theory of Ostwald Ripening. *J. Stat. Phys.* **1985**, 38 (1–2), 231–252.
- (75) Malhotra, A. K.; Wasan, D. T. Effect of Film Size on Drainage of Foam and Emulsion Films. AIChE J. 1987, 33 (9), 1533–1541.
- (76) Danov, K. D. Effect of Surfactants on Drop Stability and Thin Film Drainage. Fluid Mechanics of Surfactant and Polymer Solutions **2004**, 1–38.
- (77) García-Río, L.; Leis, R.; Mejuto, J. C.; Peña, M. E.; Iglesias, E. Effects of Additives on the Internal Dynamics and Properties of Water/AOT/Isooctane Microemulsions. *Langmuir* **1994**, *10* (6), 1676–1683.
- (78) Leung, R.; Shah, D. O. Solubilization and Phase Equilibria of Water-in-Oil Microemulsions. II. Effects of Alcohols, Oils, and Salinity on Single-Chain Surfactant Systems. *J. Colloid Interface Sci.* 1987, 120 (2), 330–344.
- (79) Jaiswal, M.; Dudhe, R.; Sharma, P. K. Nanoemulsion: An Advanced Mode of Drug Delivery System. 3 *Biotech.* **2015**, 5 (2), 123–127.
- (80) Koroleva, M.; Nagovitsina, T.; Yurtov, E. Nanoemulsions Stabilized by Non-Ionic Surfactants: Stability and Degradation Mechanisms. *Phys. Chem. Chem. Phys.* **2018**, 20 (15), 10369–10377.
- (81) Yekeen, N.; Manan, M. A.; Idris, A. K.; Samin, A. M. Influence of Surfactant and Electrolyte Concentrations on Surfactant Adsorption and Foaming Characteristics. *J. Pet. Sci. Eng.* **2017**, *149*, 612–622.
- (82) Xu, Q.; Nakajima, M.; Ichikawa, S.; Nakamura, N.; Roy, P.; Okadome, H.; Shiina, T. Effects of Surfactant and Electrolyte

Concentrations on Bubble Formation and Stabilization. J. Colloid Interface Sci. 2009, 332 (1), 208–214.

# **□** Recommended by ACS

# Impact of Particle Sedimentation in Pendant Drop Tensiometry

Roy J. B. M. Delahaije, Jack Yang, et al.

AUGUST 09, 2022

LANGMUIR

READ 🗹

# Complex Suspended Janus Droplets Constructed through Solvent Evaporation-Induced Phase Separation at the Air-Liquid Interface

Zesheng Hua, Jianfeng Li, et al.

SEPTEMBER 01, 2022

LANGMUIR

READ 🗹

# **Optical Properties of Pickering Emulsions and Foams**

Mizuho Ono, Hiroki Gonome, et al.

JANUARY 19, 2022

LANGMUIR

READ 🗹

# Investigation of the Contact Angle and Packing Density of Silica Nanoparticles at a Pickering Emulsion Interface Fixed by UV Polymerization

Jianan Xu, To Ngai, et al.

MARCH 31, 2022

LANGMUIR

READ 🗹

Get More Suggestions >